

Evaluation of Melting and Crystalline Relaxation Temperatures of Fatty Acid Monolayers on the Water Surface and Their Importances for Molecular Aggregation States in Monolayers

Tisato KAJIYAMA,* Yushi OISHI, Motoko UCHIDA, Naoaki MOROTOMI,
Jun-ichi ISHIKAWA, and Youichi TANIMOTO

Department of Chemical Science and Technology, Faculty of Engineering,
Kyushu University, 6-10-1 Hakozaki, Higashi-ku, Fukuoka 812

(Received November 7, 1991)

The melting temperature, T_m and the crystalline relaxation temperature, $T\alpha_c$ of fatty acid monolayers on the water surface were evaluated by a combination of two kinds of measurements, the subphase temperature, T_{sp} dependence of monolayer modulus based on a π - A isotherm and also, the T_{sp} dependence of the electron diffraction, ED patterns of monolayer. T_m s of myristic, palmitic, and stearic acid monolayers were evaluated to be 278, 301, and 317 K, respectively, on the basis of both apparent decrease in the T_{sp} vs. modulus curve and the change of the ED pattern from a crystalline Debye ring to an amorphous halo. The crystalline relaxation process corresponds to a change from elastic to viscoelastic characteristics in a crystalline phase due to a considerable contribution of anharmonic thermal molecular vibration. $T\alpha_c$ s of palmitic and stearic acid monolayers were evaluated to be 291 and 298 K, respectively, from both apparent decrease in the T_{sp} dependence of modulus and appearance of the break in the thermal expansion coefficient of crystalline lattice constant. This break may be attributed to a remarkable increase in contribution of the anharmonic term with respect to the intermolecular potential energy. The magnitude of T_m and $T\alpha_c$ of monolayers on the water surface is an important factor to decide the structure or aggregation state in the crystalline and amorphous monolayers and also, the formation process of a large-area monolayer, that is, the fusion or sintering behavior among crystalline monolayer domains.

Langmuir-Blodgett (LB) films constructed by successive depositions of monolayers encounter increasing interests due to many possible applications.¹⁾ Construction of defect-free monolayers is required to attain ultimate functional properties of LB films. One of effective treatments for structural ordering of monolayer is recrystallization or annealing, which is strongly related to various kinds of thermal molecular motions. Therefore, it is important to investigate the temperature dependences of the structure and morphology of monolayers on the water surface.

It has been generally accepted from surface pressure-area (π - A) isotherms that phase transitions in the process of gas, liquid expanded, liquid condensed and solid condensed phases occur upon compressing amphiphilic molecules on the water surface.²⁾ However, it has been proposed on the basis of electron microscopic observations or X-ray diffraction measurements that two-dimensional domains in a crystalline or an amorphous solid state are grown on the water surface even at a surface pressure of 0 mN m⁻¹, in the case of spreading solutions of polydiacetylene,³⁾ fatty acids,⁴⁻⁸⁾ and fatty acid salts.⁶⁻⁹⁾ It is also recognized that the π - A isotherm represents the aggregating process of domains.^{3-5,9)} These experimental results indicate that the monolayer phase on the water surface such as gas, liquid expanded and so on can not be determined only from the shape of π - A isotherm.

An electron diffraction (ED) study is one of effective techniques to investigate the monolayer phase on the water surface, if the monolayer on the water surface can be transferred onto a substrate without any phase or crystallographical change. Furthermore, thermal mo-

lecular motions in the monolayer on the water surface can be studied from the thermomechanical measurement, that is, the subphase temperature, T_{sp} dependence of the two-dimensional modulus which is evaluated by the derivative of π with respect to A .¹⁰⁾ Combination of thermomechanical and structural analyses must be an effective and quite reliable technique to investigate the thermal behavior, the melting temperature, T_m or the crystalline relaxation temperature, $T\alpha_c$ and also, the aggregation state of monolayer on the water surface.

In this paper, T_m s and $T\alpha_c$ s of the monolayers of myristic, palmitic, and stearic acids on the water surface were evaluated from the T_{sp} dependences of their moduli and ED patterns. It will be shown that the monolayer of fatty acid on the water surface can be classified simply into the two types of crystalline or amorphous monolayers, depending on the magnitude of T_{sp} in comparison with T_m or $T\alpha_c$.

Experimental

Monolayer Preparation. Myristic (C₁₄), palmitic (C₁₆), and stearic (C₁₈) acids (chromatographic reference quality) were used without further purification. Benzene with spectroscopic quality was used as solvent. Benzene solutions of myristic, palmitic, and stearic acids were prepared with concentrations of 3.7×10^{-3} , 2.8×10^{-3} , and 2.2×10^{-3} mol dm⁻³, respectively. The subphase water was purified by the Milli-QII® system (Millipore Co., Ltd.). The subphase temperature, T_{sp} was varied in a temperature range of 274–321 K by circulating constant-temperature water around an aluminum support of a trough. The accuracy of T_{sp} was ± 1 K, which was evaluated by using a thermocouple positioned ca. 1 mm below the water surface. And also, the room temperature was adjusted to the same temperature as T_{sp} by using an air-conditioner and three

infrared radiation lamps. Each monolayer was compressed to a given surface pressure at a barrier speed of 48 mm min⁻¹.

Modulus Measurement of Monolayer. π - A isotherms were obtained at various T_{sp} s with a microprocessor-controlled film balance system (FSD-20, Sanesu Keisoku Co., Ltd.). The static elasticity, K_S of monolayer on the water surface was evaluated from the π - A isotherm by using the following equation.^{10,11)}

$$K_S = -A(d\pi/dA)$$

Figure 1 shows the π - A (solid line) and the $\log K_S$ - A (broken line) isotherms for the stearic acid monolayer at T_{sp} of 293 K. $\log K_{S(max)}$ was defined as the maximum of $\log K_S$ which corresponds to the collapsing point. At this point, even though the collapsed monolayer fragments were observed as an appearance of patchy pattern on the base monolayer (the substrate monolayer on the water surface), molecules in the base monolayer were packed most densely and homogeneously. Therefore, it is reasonable to consider that homogeneous compression force was transmitted throughout the monolayer. Then, in this paper, the temperature dependence of $\log K_{S(max)}$ was adopted for determination of the melting temperature, T_m and the crystalline relaxation temperature, $T_{\alpha c}$ of monolayer on the water surface.

Substrate Preparation. The hydrophilic SiO substrate (static water contact angle: $\theta=30^\circ$), was prepared by vapor-deposited SiO onto a Formvar substrate,¹²⁾ with which an electron microscope grid (200-mesh) was covered. The relatively hydrophobic siliconized substrate ($\theta=90^\circ$) was also prepared by surface siliconized treatment; a collodion-covered electron microscope grid was dipped into an aqueous solution of silane coupling agent.

Electron Microscopic Observation. Bright field electron micrographs and ED patterns were taken with a Hitachi H-500 electron microscope, which was operated at an acceleration voltage of 75 kV and a beam current of 2.5 μ A. The electron beam was 2 μ m in diameter. Electron microscopic observations were carried out at the same temperature as T_{sp} at which the monolayer was prepared on the water surface, by using a thermostating apparatus. Pt-carbon was vapor-deposited onto the monolayer samples with a shadowing angle of 25° for the bright field electron microscopic observation.

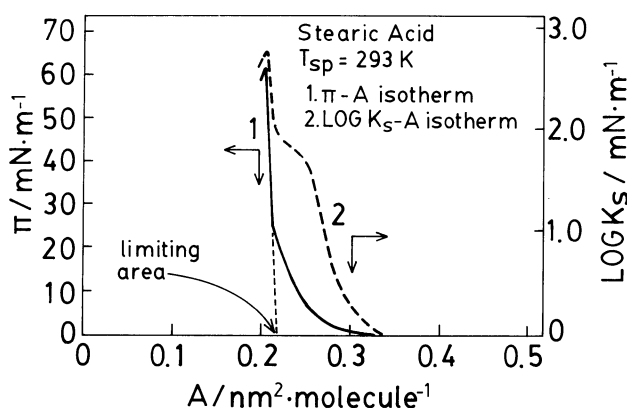


Fig. 1. The π - A and $\log K_S$ - A isotherms of the stearic acid monolayer at T_{sp} of 293 K.

Results and Discussion

Investigation of Transfer Method of Monolayer.

Figure 2 shows the ED patterns of arachidic acid monolayers transferred onto a SiO substrate (a) and a siliconized one (b) by an upward drawing method with a drawing speed of 60 mm min⁻¹ at $\pi=25$ mN m⁻¹, respectively. The hydrophilic part of the monolayer contacts with the substrate surface by the upward drawing method.

As shown in Fig. 2, the crystalline structure of the monolayer depends on the hydrophilic or hydrophobic characteristics of the substrate, may be due to the difference of interfacial interaction. The monolayer transferred on the hydrophilic substrate such as SiO shows that the crystal system of the monolayer is hexagonal. The diffraction spot of 0.42 nm spacing is assigned to the (10) reflection of two-dimensional hexagonal crystal. This hexagonal crystal system agrees with that of the arachidic acid monolayer on the water surface, which was confirmed by a grazing incidence in-plane X-ray diffraction.⁸⁾ Since the hydrophilic group of the monolayer contacts with the hydrophilic SiO substrate during transfer of the monolayer, this interfacial condition is in a similar fashion to that of the monolayer on the water surface with respect to the magnitude of interfacial free energy between the hydrophilic(polar) group of monolayer and the hydrophilic substrate surface. Therefore, it is reasonable to consider that the hexagonal crystal system of the monolayer on the water surface is transferred and stably maintained on the hydrophilic substrate.

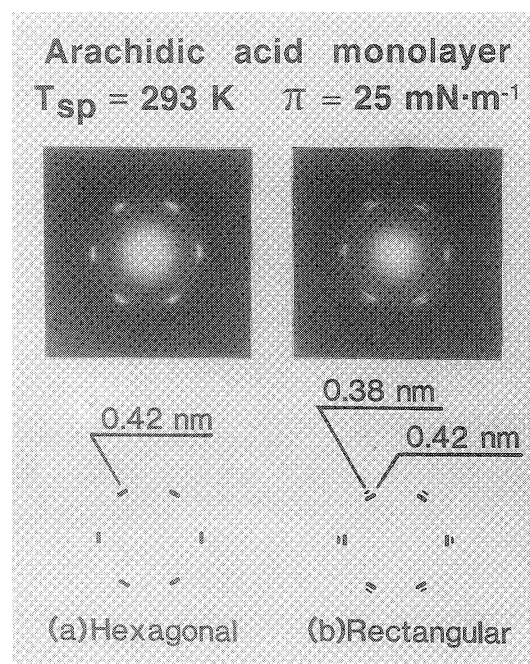


Fig. 2. The ED patterns of the arachidic acid monolayers transferred onto (a) SiO and (b) silicone substrates.

On the other hand, the ED pattern of Fig. 2(b) shows that the crystal system of the arachidic acid monolayer transferred on the siliconized hydrophobic substrate is face-centered rectangular. The diffraction spots of 0.42 and 0.38 nm spacings are assigned to the (11) and (20) reflections of the two-dimensional rectangular crystal, respectively. The hexagonal crystal system on the water surface could not be transferred and maintained on the siliconized hydrophobic substrate because the surface energy of the substrate was quite different from that of the water surface. In this case, since the interfacial interaction between the hydrophilic(polar) group of the monolayer and the hydrophobic substrate surface becomes weaker with an increase in the surface energy difference, fatty acid molecules form their inherent crystalline structure. Then, it seems reasonable to conclude from Figs. 2(a) and 2(b) that the crystalline structure of fatty acid monolayers on the water surface can be transferred onto a hydrophilic substrate by the upward drawing method without any change of crystallographical system. Also, since the surface of the hydrophilic SiO substrate in an amorphous state is quite smooth, the SiO substrate is suitable for the electron microscopic observation of the monolayer without any change of the crystallographical structure of the monolayer on the water surface. Then, in order to investigate the thermal behavior of the monolayer structure on the water surface, the monolayer was transferred onto the hydrophilic SiO substrate by the upward drawing method with the drawing speed of 60 mm min^{-1} at various T_{sp} s and at a certain surface pressure where each monolayer was morphologically homogeneous.⁴⁾

Determination of Melting Temperature of Monolayer on the Water Surface. Figure 3 shows the T_{sp} dependences of $\log K_{\text{S(max)}}$ for stearic acid monolayer on the

water surface and the ED patterns of the monolayer transferred onto the hydrophilic substrate at the surface pressure of 20 mN m^{-1} . The homogeneous monolayer was formed on the water surface at this magnitude of surface pressure. The ED patterns were taken at the same temperature as T_{sp} at which the monolayer was prepared. The magnitude of $\log K_{\text{S(max)}}$ started to apparently decrease at ca. 298 and 317 K. The ED patterns at 313 and 319 K were a crystalline Debye ring and an amorphous halo, respectively. Therefore, Figure 3 indicates that a fairly remarkable decrease of $\log K_{\text{S(max)}}$ at around 317 K corresponds to the melting behavior of stearic acid monolayer on the water surface. Also, T_{ms} of palmitic and myristic acid monolayers on the water surface were similarly estimated to be 301 and 278 K, respectively, on the basis of the T_{sp} dependence of $\log K_{\text{S(max)}}$ and ED patterns as shown in Figs. 4 and 5.¹³⁾ As mentioned above, T_{m} of the fatty acid monolayer on the water surface is successfully evaluated from the T_{sp} dependences of static elasticity and ED pattern.

Figure 6 shows variation of T_{ms} for the fatty acid monolayers on the water surface (1), three-dimensional crystals (2), and normal paraffins (3)¹⁴⁾ with the number of corresponding carbon atom in an alkyl chain. T_{ms} of myristic (C_{14}), palmitic (C_{16}), and stearic (C_{18}) acid monolayers are ca. 278, 301, and 317 K, respectively, as determined from Figs. 3–5. It is difficult to evaluate T_{ms} of fatty acid monolayers with alkyl chain longer than C_{18} due to an experimental limitation with respect to increasing T_{sp} (heating the LB trough) and also, heating the monolayer samples in an electron microscope. T_{ms} of the fatty acid monolayers are much lower than those of corresponding three-dimensional crystals (2: bulk) because the monolayer is thermodynamically less stable than the three-dimensional crystal. However, the magnitude difference between T_{ms} for monolayer and

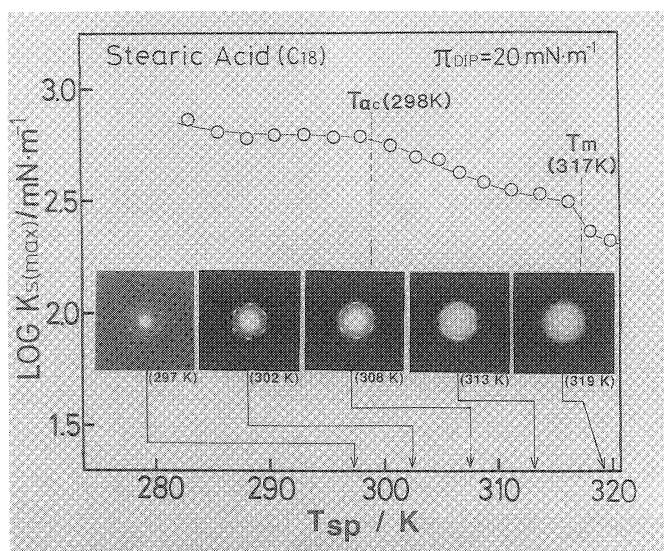


Fig. 3. The T_{sp} dependences of $\log K_{\text{S(max)}}$ and ED patterns of the stearic acid monolayers.

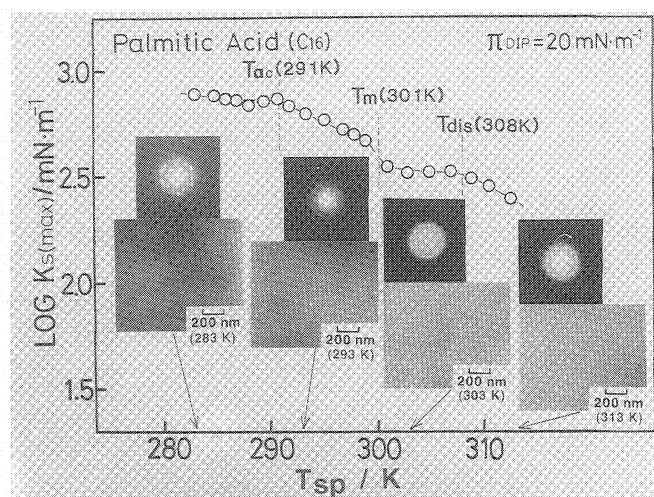


Fig. 4. The T_{sp} dependences of $\log K_{\text{S(max)}}$, bright field electron micrographs and ED patterns of the palmitic acid monolayers.

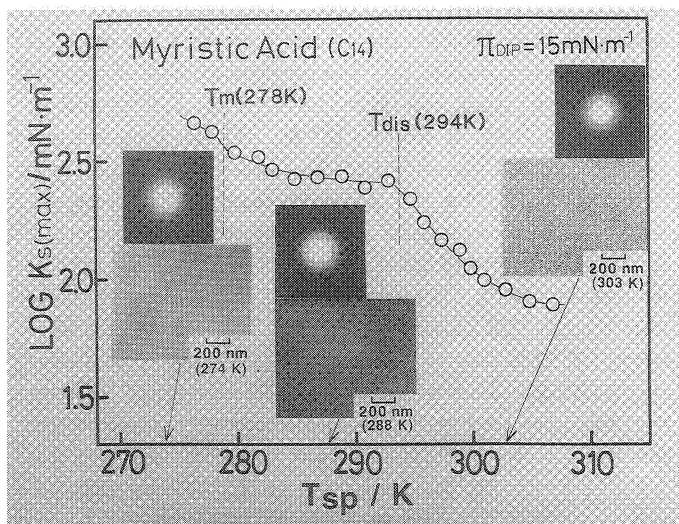


Fig. 5. The T_{sp} dependences of $\log K_{S(max)}$, bright field electron micrographs and ED patterns of the myristic acid monolayers.

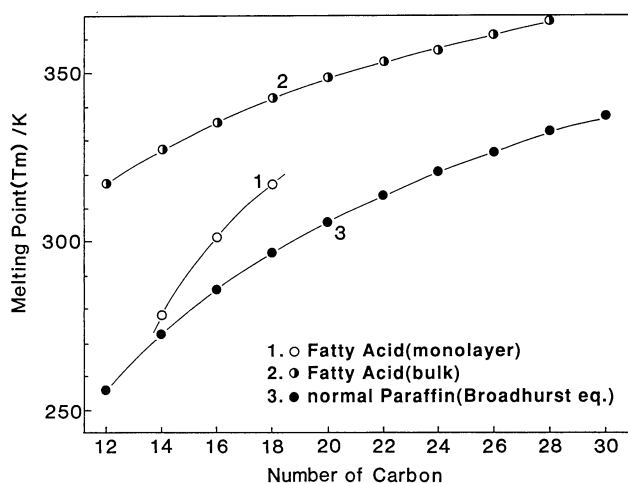


Fig. 6. Variation of T_m with alkyl chain length for (1) fatty acids in a monolayer state, (2) fatty acids in a three-dimensional crystalline state, and (3) normal paraffins in a three-dimensional crystalline state.

bulk crystal becomes smaller with an increase in alkyl chain length. This indicates that intermolecular aggregation force in a monolayer state increases with increasing alkyl chain length.¹⁵⁾

As mentioned later (Fig. 8), T_m was also confirmed from the limiting area vs. T_{sp} curve since the magnitude of the limiting area jumps in the temperature range of T_m due to a remarkable increase of the molecular occupied area in a melt state.

New Concept on Crystalline Relaxation Process in Monolayer. Figure 3 shows that the slope of $\log K_{S(max)}$ vs. T_{sp} curve for the stearic acid monolayer slightly decreased at ca. 298 K which was denoted by T_{α_c} . In a T_{sp} range below 298 K, the ED pattern of the stearic acid

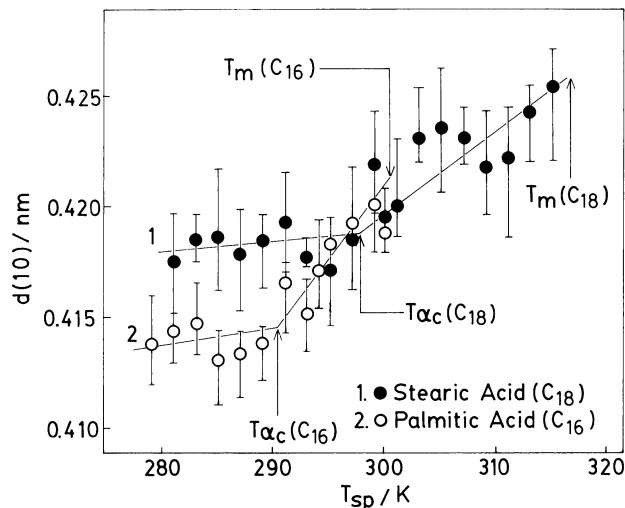


Fig. 7. The T_{sp} dependences of the (10) spacing of the stearic and the palmitic acid monolayers.

monolayer exhibited sharp crystalline spots with spacings of 0.42 and 0.24 nm. Since the ratio of reciprocal spacings is $1:\sqrt{3}$, stearic acid molecules are packed in a hexagonal unit cell and these diffraction spots are assigned to (10) and (11) reflections, respectively. In contrast, in a T_{sp} range above 298 K, the ED spots tended to be more arc along an azimuthal direction and also, to be broader with an increase of T_{sp} , resulting in the Debye ring. This indicates that the orientation of stearic acid molecules and/or crystalline domains become broader or less regular with an increase in T_{sp} above ca. 298 K. In the case of the palmitic acid monolayer, similar behaviors with respect to the T_{sp} dependence of $\log K_{S(max)}$ and ED patterns were observed in T_{sp} ranges below and above 291 K, as shown in Fig. 4.

Figure 7 shows the T_{sp} dependences of the (10) spacing evaluated from the ED patterns of the stearic and the palmitic acid monolayers. Hereupon, it should be reminded that the ED pattern was taken at the same temperature as T_{sp} , by warming up the sample chamber in an electron microscope. The (10) spacing vs. T_{sp} curve exhibited a distinct break at ca. 298 and 291 K for the stearic and the palmitic acid monolayers, respectively, though the values of the (10) spacing were fairly scattered. Then, the temperature range of the break point on the (10) spacing vs. T_{sp} curve apparently corresponds to that for an apparent decrease of $\log K_{S(max)}$ as shown in Figs. 3 and 4. The T_{sp} dependence of $\log K_{S(max)}$ is very similar to that of the crystalline relaxation behavior of which the mechanical crystalline relaxation mechanisms were extensively studied for a single crystal mat and a spherulitic film of high density polyethylene (PE).¹⁶⁻¹⁸⁾ The lateral attractive force between PE chains in the crystal lattice is fairly weaker compared with the covalent bonding force along a PE chain. Therefore, the rotational oscillation about

a PE chain readily occurs across the intermolecular energy barrier in a higher temperature range at which the oscillations of neighboring chains are incoherent. This causes an increase of anharmonicity for the intermolecular potential energy, which was confirmed^{19,20)} by an increase in Grüneisen constant evaluated from the pressure dependence of sound velocity and compressibility. Therefore, a remarkable increase in anharmonicity on intermolecular potential energy causes an increase in viscous contribution to the viscoelastic characteristics in a crystalline region and also, an apparent change on the thermal expansion of the lattice spacing. This kind of viscoelastic characteristics in a crystalline region was designated the crystalline relaxation behavior. Consequently, it is reasonable to conclude from Figs. 3, 4, and 7 that the viscoelastic crystalline relaxation behaviors were newly confirmed even in the crystalline stearic and palmitic acid monolayers.

Figure 8 shows the T_{sp} dependence of the limiting area

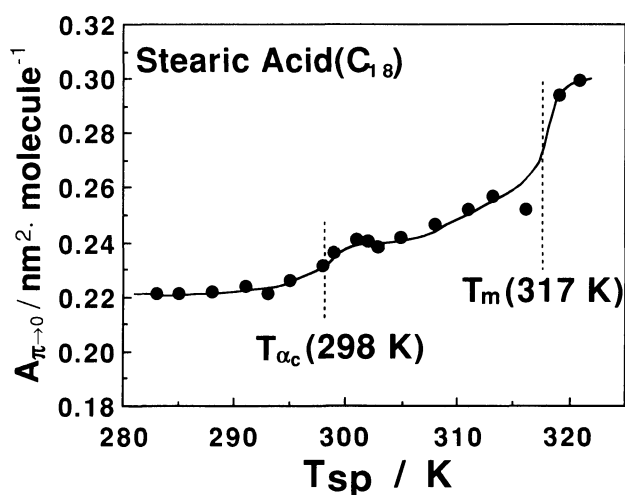
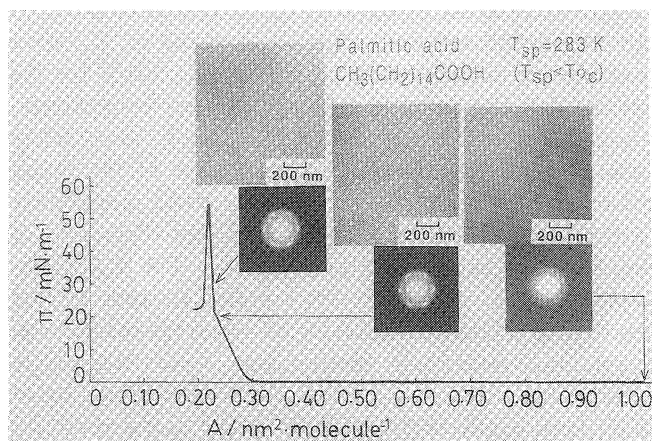


Fig. 8. The T_{sp} dependence of the limiting area for the stearic acid monolayers.

(a)



for the stearic acid monolayer. The limiting area was obtained from the extrapolation of the π -A isotherm to $\pi=0$, as shown in Fig. 1. The limiting area vs. T_{sp} curve exhibited a slight increase at around 298 K and a remarkable one at about 317 K. These temperature ranges well corresponded to T_{α_c} and T_m for the stearic acid monolayer on the water surface, respectively, as shown in Figs. 3, 6, and 7. It may be considered that increase of limiting area at around 298 and 317 K occur in accordance with increases in the thermal expansion coefficient of the crystal lattice and also, in the molecular occupied area due to the solid-liquid phase transition, respectively. Therefore, the T_{sp} dependence of the limiting area of Fig. 8 is a supplementary support for determination of T_{α_c} and T_m for the monolayer on the water surface on the basis of the T_{sp} dependences of $\log K_{S(\text{max})}$ and ED pattern as shown in Fig. 3.

Then, it seems reasonable to conclude that the counterpart investigation on the T_{sp} dependence of $\log K_{S(\text{max})}$ and also, ED pattern for the monolayer which was transferred onto a hydrophilic substrate is quite reliable to determine the magnitudes of T_{α_c} and T_m of the monolayer on the water surface.

Melting Temperature-Aggregation Structure Relationships of Monolayers. Figure 9(a) shows the π -A isotherm for the palmitic acid monolayer spread on the water surface at T_{sp} of 283 K which was much lower than T_m of the monolayer, as well as the bright field images and the ED patterns of the monolayers which were transferred onto the hydrophilic SiO substrate at surface pressures of 0, 20, and 30 $\text{mN} \cdot \text{m}^{-1}$. The π -A isotherm showed a sharp rise of surface pressure with decreasing the surface area without any appearance of a plateau region. At 0 $\text{mN} \cdot \text{m}^{-1}$, many isolated domains were observed in the bright field image. The bright field image of the monolayer transferred at 20 $\text{mN} \cdot \text{m}^{-1}$ exhibited the fairly uniform, smooth and continuous morphology. Also, the bright field image at 30 $\text{mN} \cdot \text{m}^{-1}$ showed a heterogeneous aggregation which was com-

(b)

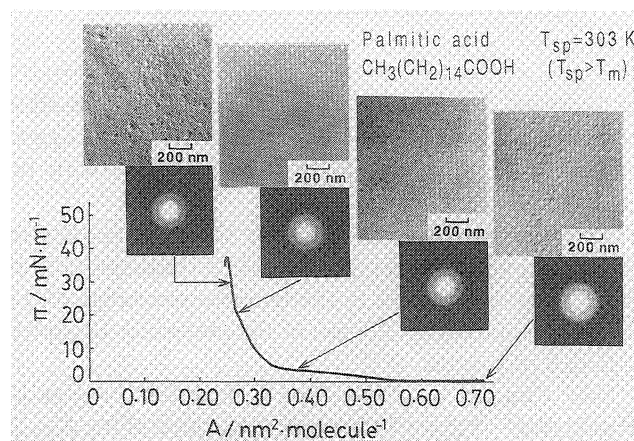


Fig. 9. The π -A isotherms, the electron micrographs and the ED patterns of the palmitic acid monolayers at T_{sp} of 283 K below T_m (a) and 303 K above T_m (b).

posed of partially patched domains due to the collapse of the monolayer. This indicates that partial collapse occurs at a lower surface pressure than the generally defined collapsed pressure as the peak of the π - A isotherm. The collapse behavior is similar to that for the barium stearate monolayer.⁹⁾ The ED pattern of the monolayer transferred at 0 mN m⁻¹ exhibited a crystalline Debye ring. Therefore, the monolayer domains observed in the bright field image at 0 mN m⁻¹ are in a crystalline state and also, orient randomly along their crystallographic axes. On the other hand, the ED patterns at 20 and 30 mN m⁻¹ showed crystalline hexagonal spots. This suggests that crystalline domains in a fairly large area (corresponding to an electron beam diameter of 2 μ m) were fused or recrystallized at the lateral surfaces, resulting in the formation of a large area monodomain monolayer, owing to sintering behavior caused by higher surface pressure below T_{α_c} . It has been reported that the crystalline ED spots of the behenic acid monolayer became sharper, along an azimuthal direction with time when the monolayer was maintained at a constant surface area after being compressed to a surface pressure of 32 mN m⁻¹ at T_{sp} below T_{α_c} .²¹⁾ This indicates the time-dependent alignment or ordering of crystallographic axes of crystalline domains in the monolayer due to sintering at the lateral interface. Thus, since sintering behavior is a kinetic one, sintering between domains in a crystalline state during compression of the monolayer at T_{sp} below T_{α_c} may depend on the compression speed. The electron microscopic study in Fig. 9(a) indicates that small two-dimensional crystalline domains grow right after spreading a solution on the water surface and aggregate together with aligning their crystallographic axes during the process of surface compression. This molecular aggregation type was designated the crystalline monolayer.

Figure 9(b) shows the π - A isotherm for the palmitic acid monolayer spread on the water surface at T_{sp} of 303 K above T_m of the monolayer, together with the bright field images and the ED patterns of the monolayers being transferred on the hydrophilic SiO substrate at 0, 5, 20, and 30 mN m⁻¹. A plateau region of the π - A isotherm was observed in a surface area range of 0.50–0.30 nm² molecule⁻¹. At 0 mN m⁻¹, the bright field image and the ED pattern of the monolayer showed an island structure and an amorphous halo, respectively. Therefore, the electron microscopic studies indicate that isolated amorphous domains are grown right after spreading a solution on the water surface and aggregate during a compressing process. Even though the monolayer was compressed up to the so-called collapsing pressure of about 37 mN m⁻¹ at T_{sp} above T_m , the monolayer was still in an amorphous state without any phase transition from an amorphous state to a crystalline one. This molecular aggregation type was designated the amorphous monolayer.

It is clear from Figs. 9(a) and 9(b) that the aggregation

structure of the palmitic acid monolayer is decisively determined by the magnitude of T_{sp} relatively above or below T_m . This conclusion may be adopted to the almost all case of fatty acid. Thus, the evaluation of T_m of the monolayer on the water surface is very important to classify systematically the aggregation state of monolayer. Furthermore, structural classification of the monolayer made us expect possibility for construction of a large two-dimensional single crystal monolayer, for example, by cooling the amorphous monolayer on the water surface down to a temperature range below T_m of the monolayer.²²⁾

Influence of Crystalline Relaxation Behaviors on Aggregation Structure of Monolayers. Figure 10 shows the π - A isotherm of the palmitic acid monolayer which was prepared at T_{sp} of 293 K between T_{α_c} and T_m , as well as the bright field images and the ED patterns of the monolayer which were transferred onto the hydrophilic SiO substrate at 0, 20, and 35 mN m⁻¹. The bright field image and the ED pattern of the monolayer at 0 mN m⁻¹ showed an island structure and a crystalline Debye ring, respectively. With increasing a surface pressure, the bright field images exhibited the gathering process of the monolayer islands, while every ED pattern showed a Debye ring. These results clearly indicate that the two-dimensional crystalline domains are grown right after spreading a solution on the water surface and gathered together during a process of surface compression, without any orientational change of crystallographic axes. In the case of T_{sp} below T_{α_c} as shown in Fig. 9(a), the crystalline monolayer domains were gathered, aligning their crystallographic axes during a process of surface compression, that is, a surface pressure-induced orientation. Therefore, in comparison of Fig. 9(a) with Fig. 10, the crystalline relaxation process is apparently important to form a large-area crystalline monolayer which are induced by a sintering behavior at the interface between crystalline domains.

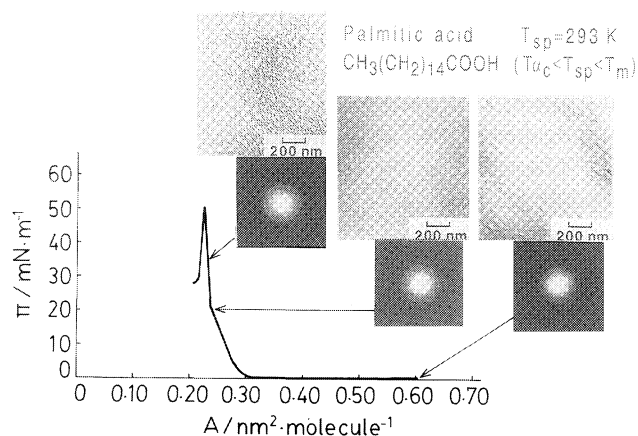


Fig. 10. The π - A isotherms, the electron micrographs and the ED patterns of the palmitic acid monolayers at T_{sp} of 293 K between T_{α_c} and T_m .

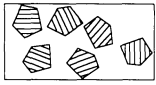

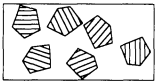
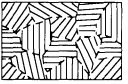
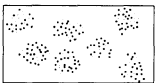

| | Subphase Temp., T_{sp} | Morphological Structure | |
|-----------------------|-------------------------------|---|---|
| | | $\pi = 0$ | $\rightarrow \pi = \pi_{dip}$ |
| Crystalline monolayer | $T_{sp} < T_{\alpha_c}$ |  |  |
| | $T_m > T_{sp} > T_{\alpha_c}$ |  |  |
| Amorphous monolayer | $T_{sp} > T_m$ |  |  |

Fig. 11. Aggregation type of fatty acid monolayer on the water surface.

Systematic Classification of Aggregation Structure of Fatty Acid Monolayers. Figure 11 shows the schematic representation of the systematic classification of the aggregation structure of fatty acid monolayers on the water surface. Fatty acid monolayers can be classified into the crystalline and amorphous monolayers, depending on T_{sp} below and above T_m , respectively. The crystalline monolayer can be further classified: crystalline domains are aligned along their crystallographic axes by surface compression at T_{sp} below T_{α_c} , while not above T_{α_c} .

In the case of T_{sp} below T_{α_c} , isolated two-dimensional crystalline domains are formed at 0 mN m^{-1} , without alignment of their crystallographic axes. With increasing surface pressure, these crystalline domains are gathered together into morphologically homogeneous state, with alignment of their crystallographic axes, owing to sintering among crystalline domains.

In the case of T_{sp} above T_{α_c} and below T_m , crystalline domains formed at 0 mN m^{-1} are gathered together into morphologically homogeneous state by surface compression, without alignment of their crystallographic axes, owing to the prevention of sintering among crystalline domains by the active thermal molecular motion above T_{α_c} .

At T_{sp} above T_m , isolated amorphous domains formed at 0 mN m^{-1} are gathered together into morphologically homogeneous state at higher surface pressures, without any phase transition from an amorphous state to a crystalline one.

Conclusion

The melting temperature, T_m and the crystalline relaxation temperature, T_{α_c} of the fatty acid monolayers on the water surface could be evaluated from the subphase temperature, T_{sp} dependences of modulus and ED pattern of the monolayer which was transferred onto a hydrophilic surface. The molecular aggregation type of the monolayer such as a crystalline monolayer and an amorphous one could be designated systematically on the

basis of the relative magnitude of T_{sp} to T_m of the monolayer (T_{sp} below or above T_m). Therefore, a surface pressure-induced phase transition from an amorphous state to a crystalline one was not observed during a compression process. A surface pressure-induced orientation of crystalline domains was observed during a compression process of monolayer at T_{sp} below T_{α_c} , while not at T_{sp} between T_{α_c} and T_m . The crystalline relaxation process is important to prepare a large-area monolayer with an excellent crystallographic orientation by sintering an interface region between the crystalline monolayer domains.

References

- 1) G. G. Roberts, *Adv. Phys.*, **34**, 475(1985).
- 2) G. L. Gaines, Jr., "Insoluble Monolayers at Liquid-Gas Interface," Interscience, New York (1966).
- 3) B. Tieke and K. Weiss, *J. Colloid Interface*, **101**, 129 (1984).
- 4) T. Kajiyama, Y. Tanimoto, M. Uchida, Y. Oishi, and R. Takei, *Chem. Lett.*, **1989**, 189.
- 5) N. Uyeda, T. Takenaka, K. Aoyama, M. Matsumoto, and Y. Fujiyoshi, *Nature*, **327**, 319 (1987).
- 6) P. Dutta, J. B. Peng, B. Lin, J. B. Ketterson, and M. Prakash, *Phys. Rev. Lett.*, **58**, 2228 (1987).
- 7) H. Möhwald, *Angew. Chem., Int. Ed. Engl.*, **27**, 728 (1988).
- 8) K. Kjaer, J. Als-Nielsen, C.A. Helm, P. Tippman-Krayer, and H. Möhwald, *J. Phys. Chem.*, **93**, 3200 (1989).
- 9) T. Kajiyama, K. Umemura, M. Uchida, Y. Oishi, and R. Takei, *Bull. Chem. Soc. Jpn.*, **62**, 3004 (1989).
- 10) T. Kajiyama, N. Morotomi, M. Uchida, and Y. Oishi, *Chem. Lett.*, **1989**, 1047.
- 11) Y. L. Chen, M. Sano, M. Kawaguchi, H. Yu, and G. Zograf, *Langmuir*, **2**, 349 (1986).
- 12) S. Fereshtekhou, R. D. Neuman, and R. Ovalle, *J. Colloid Interface Sci.*, **109**, 385 (1986).
- 13) The log $K_{S(\max)}$ for palmitic and myristic acid monolayers decreased also at T_{sp} s of 308 and 294 K, as shown in Figs. 4 and 5, respectively. This may be due to dissolution of palmitic and myristic acid molecules into the water phase in temperature ranges above T_{sp} s of 308 and 294 K, respectively.
- 14) M. G. Broadhurst, *J. Res. Natl. Bur. Stand., Sect. A*, **70**, 481 (1966).
- 15) T. Kajiyama, I. Hanada, K. Shuto, and Y. Oishi, *Chem. Lett.*, **1989**, 193.
- 16) M. Takayanagi and M. Matsuo, *J. Macromol. Sci., Phys.*, **B1**, 407 (1967).
- 17) T. Kajiyama, T. Okada, A. Sakoda, and M. Takayanagi, *J. Macromol. Sci., Phys.*, **B7**, 583 (1973).
- 18) T. Kajiyama, M. Kuroishi, and M. Takayanagi, *J. Macromol. Sci., Phys.*, **B11**, 121 (1975).
- 19) T. Kijima, K. Koga, K. Imada, and M. Takayanagi, *J. Macromol. Sci., Phys.*, **B10**, 709 (1974).
- 20) T. Kijima, K. Koga, K. Imada, and M. Takayanagi, *Polym. J.*, **7**, 14 (1975).
- 21) T. Tanizaki, A. Takahara, and T. Kajiyama, *J. Soc. Rheol., Jpn.*, **19**, 208 (1991).
- 22) T. Kajiyama, K. Umemura, M. Uchida, Y. Oishi, and R. Takei, *Chem. Lett.*, **1989**, 1515.